Nanoscale

Accepted Manuscript

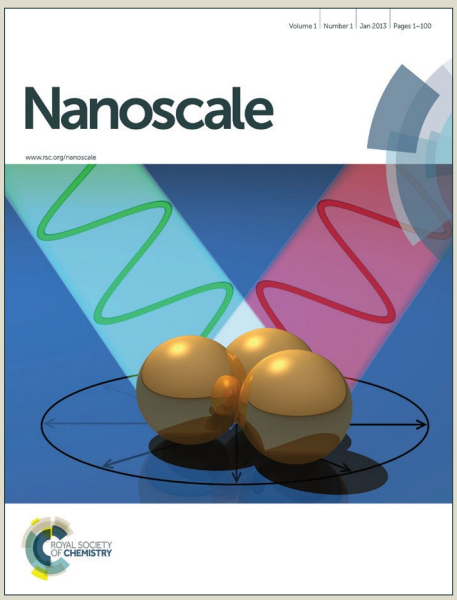

ROYAL SOCIETY OF CHEMISTRY

www.rsc.org/nanoscale

Nanoscale

RSCPublishing

PAPER

Gigantic Enhancement in Dielectric Properties of Polymer-based Composites Using Core/Shell MWCNT/Amorphous Carbon Nanohybrid

Qikai Guo[ab], Qingzhong Xue[*ab], Jin Sun[b], Mingdong Dong[c], Fujun Xia[b], and Zhongyang Zhang[b]

Novel core/shell structured multi-walled carbon nanotube/amorphous carbon (MWCNT@AC) nanohybrids were successfully prepared by a simple and novel method. And then the MWCNT@AC nanohybrids were used as fillers to enhance the dielectric properties of poly(vinylidene fluoride) (PVDF) based composites. It is found that the dielectric constant of MWCNT@AC/PVDF composites can reach 5910 (the dielectric loss is ~2), which is much better than that of MWCNT/PVDF composites. The uniform amorphous carbon shell provides an insulative layer between adjacent MWCNTs in polymer matrix, which not only prevents the direct contact of MWCNTs but also improves the dispersibility of MWCNTs. Therefore, a surprising number of microcapacitors could be formed in composites before the formation of conductive network, leading to a gigantic enhancement in dielectric properties. Our strategy provides a new idea to fabricate excellent dielectric materials for energy storage capacitors and the design concept used in this work can be extended to other carbon materials.

1 Introduction

Energy storage capacitor with high energy density, which allows adequate electrical energy to be stored and released under controlled conditions,[1,2] has attracted significant attention for their application in many fields, such as portable electronics,[3] hybrid electric vehicles,[4] and pulse power applications.[5] According to the capacitor theory,[6] the energy density of capacitors is mainly dependent on the corresponding dielectric materials. Therefore, the development of excellent dielectric materials has become a research focus.[7-9] Recently, polymer has been used as dielectric material for capacitors, due to its high electric breakdown field, low dielectric loss, and easy processing.[10] However, the dielectric constant of common polymers is very low (i.e., <10), which limits their charge storage capacity.[11]

Fortunately, people have found that the dielectric constant of polymer can be greatly enhanced by adding conductive fillers (e.g., metal nanoparticles, carbon black, graphene, and carbon nanotubes) into polymer matrix,[12-17] which can be explained by an adopted microcapacitor model.[18] Based on this model, the polymer-based composites can be simulated by a large equivalent microcapacitor network, where the adjacent conductive fillers serve as the electrodes and the polymer matrix between them serves as dielectrics.[19] Each microcapacitor contributes an abnormally large capacitance. The large capacitance contributed by each of these microcapacitors can then be correlated with a significant increase in the dielectric constant of composites,[20] which indicates the number of microcapacitors taking a dominate role in the dielectric properties. However, according to the percolation theory, the filler loading is limited by a critical parameter, namely, percolation threshold. Once the filler loading exceeds the percolation threshold, the composites will turn to conducting materials rather than dielectrics due to the formation of conductive network.[21] Therefore, the key issue to achieve gigantic enhancement in dielectric constant of polymer-based composites is preventing the formation of conductive network.

Among these conductive fillers, carbon nanotubes (CNTs) have become a focal point of polymer-based composite research because of their high-aspect ratio and extraordinary electrical and mechanical properties.[22,23] However, the increase in dielectric constant of these polymer-based composites by adding pristine CNTs is far less than expectations.[24] One significant reason is the direct connection between pristine CNTs, which leads to the formation of conductive network at a very low CNT concentration. Microcapacitors in these composites are severely inadequate to create a high dielectric constant. For instance, Wang et al.[24] fabricated MWCNT/PVDF composites and demonstrated that the percolation threshold of the composites is loss than 1.61 vol%. As a result, the largest dielectric constant of such composite is less than 50, making it not an ideal dielectric material. In order to prevent the direct contact of adjacent CNTs, the chemical functionalization has been introduced in recent years.[16,25,26] Dang et al.[25] fabricated functionalized MWCNT/PVDF composites with a dielectric constant about 600 and a dielectric loss above 2 at the percolation threshold (f_c=8.0 vol%) by using

[a]*State Key Laboratory of Heavy Oil Processing, China University of Petroleum, Qingdao 266580, Shandong, P. R. China*

[b]*College of Science, China University of Petroleum, Qingdao 266580, Shandong, P. R. China*

[c]*Interdisciplinary Nanoscience Center (iNANO), Aarhus University, DK-8000 Aarhus C, Denmark*

E-mail:xueqingzhong@tsinghua.org.cn;duyg@upc.edu.cn

trifluorobromobenzene functionalized MWCNTs as fillers. The incorporation of organic groups can effectively reduce the connection of MWCNTs. As a result, the percolation threshold of functionalized MWCNT/PVDF composites has been greatly improved. More microcapacitors can be formed in this case resulting in an order-of-magnitude improvement in dielectric constant. However, the dielectric loss of such composites is usually high because of the avoidless direct contact among MWCNTs with high loadings. Therefore, chemical modification is not an optimal method to achieve gigantic enhancement in dielectric constant.

Another strategy is introducing interlayers or shells on the surface of CNTs by chemical vapour deposition, electrostatic interactions or in situ polymerization.[19,27-30] Zhou et al.[28] fabricated emeraldine base coated MWCNTs (MEB) with core/shell structure by in situ polymerization and studied the dielectric properties of MEB/PVDF composites. It demonstrates that the dielectric constant of such composite reaches 260 and the dielectric loss is ~1 when the concentration of fillers is 8.3 vol%. However, although the filler content has been improved, the enhancement in dielectric constant is far less than expectations. Furthermore, the methods used in this work are relatively complicated and reactants used in fabricating MEB (such as aniline and ammonium peroxydisulfate) are toxic.

In this paper, we present a very simple, environmentally friendly and effective route to fabricate polymer-based composites by employing core/shell-structured MWCNT@AC nanohybrids as fillers and PVDF as matrix. The ultrathin amorphous carbon shell (<2 nm) around the surface of MWCNT provides an insulative layer between adjacent MWCNTs, which not only prevents the direct contact of MWCNTs but also improves the dispersibility of MWCNTs. Conductive network in such composites is particularly difficult to be formed even with a high MWCNT concentration (>10.4 vol%). Moreover, our approach is an absolutely "green" method. The MWCNT@AC nanohybrids were fabricated in aqueous glucose solutions by hydrothermal reaction and no toxic reagents were used.[31] All these features offer a new idea for the design of an entirely different class of dielectric materials that can be used in high energy storage capacitors.

2 Results and discussion

2.1 Synthesis mechanism of MWCNT@AC nanohybrids

In order to hold excellent electric conductivity, MWCNTs were not treated by chemical modification before hydrothermal reaction, making it difficult to disperse MWCNTs in solvent homogeneously. Therefore, surfactant and homogeneous reactor was used in experiment to solve this problem. The results indicate that the surfactant adsorbed onto the nanotube surfaces significant promotes the monodispersion of MWCNTs in suspension. Furthermore, the utilization of homogeneous reactor ensures that the hydrothermal reaction occurred under stirring and accelerates the diffusion of solutes toward MWCNTs surfaces.

The core-shell structured MWCNT@AC nanohybrids were synthesized under hydrothermal conditions at 453 K (as shown in Fig. 1), which is higher than the normal glycosidation temperature.[31] Various chemical reactions of glucose can take place during the heating process. When the glucose solution was treated below 413 K, some aromatic compounds and oligosaccharides were formed, then might be adsorbed on the surface of MWCNTs due to a π-π stacking

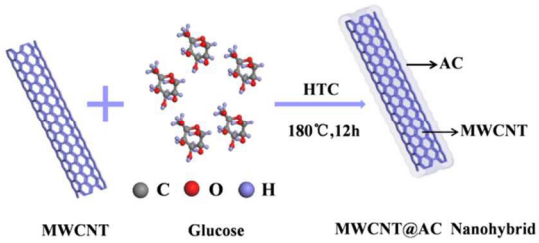

Fig. 1 Schematic diagram showing the overall fabrication process for MWCNT@AC nanohybrid.

interaction. After the solution reached a critical temperature (433 K), a continuous carbonization process resulted. At first, some adjacent aromatic compounds and oligosaccharides adsorbed on the surface of MWCNTs were cross-linked by intermolecular dehydration. Then more and more macromolecules participated in the process by diffusing solutes toward the template surfaces until the final amorphous carbon shell was attained.

2.2 Characterization of pristine MWCNTs and MWCNT@AC nanohybrids

Fig. 2 shows the TEM images of pristine MWCNTs and MWCNT@AC nanohybrids. From Fig. 2c and 2d, it can be clearly seen that MWCNTs are coated by an ultrathin shell and the thickness of the layer is below than 2 nm. The coating is fairly uniform and no bare MWCNTs are observed in Fig. 2b. Such a thin shell provides a barrier layer between adjacent MWCNTs, making the direct contact of MWCNTs impossible. When blended with polymer matrix, the dielectric properties of composites will be enhanced and the results will be discussed in the following section.

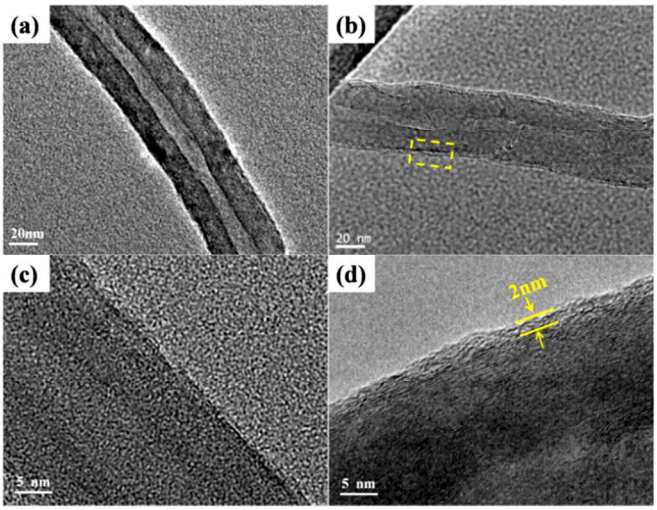

Fig. 2 TEM images of (a), (c) pristine MWCNTs and (b), (d) MWCNT@AC nanohybrids.

Raman spectroscopy analysis was performed in the range of 1100-1800 cm^{-1} in order to check the structure differences between pristine MWCNTs and MWCNT@AC nanohybrids as shown in Fig. 3. The Raman spectra were obtained using an excitation wavelength of 514.5 nm. Both specimens exhibit two peaks around 1340 and 1570 cm^{-1}, indicating the stretching modes of the D band and G band, respectively. The G-band are coming from the stretching of conjugated double bonds corresponds to sp^2 hybridization during the

formation of the aryl-nanotube bond, and the D-bands are from the multiple phonon scattering of defects.[10] The variation of the D and G peaks and the ratio of their intensity are commonly used to quantify the structural quality of MWCNT.[32,33] After fitted by mixing a Gaussian shape, it can be found that the intensity ratio of I_D/I_G in MWCNT@AC nanohybrids (0.54) decreases in comparison with that in pristine MWCNTs (0.66), which is similar to the result of Yang et al.[34] The decrease of intensity ratio in MWCNT@AC nanohybrids arises from the combined action of MWCNT core and amorphous carbon shell. Furthermore, the full-width at half-maximum (FWHM) of the D and G band can be used to determine the crystallinity degree of graphitic materials.[29] Compared with pristine MWCNTs, the D band FWHM slightly increases from 46 to 48 cm^{-1} in MWCNT@AC nanohybrids. This means that MWCNT@AC nanohybrids are a little less ordered than the pristine MWCNTs which can be attributed to the introduction of amorphous carbon.

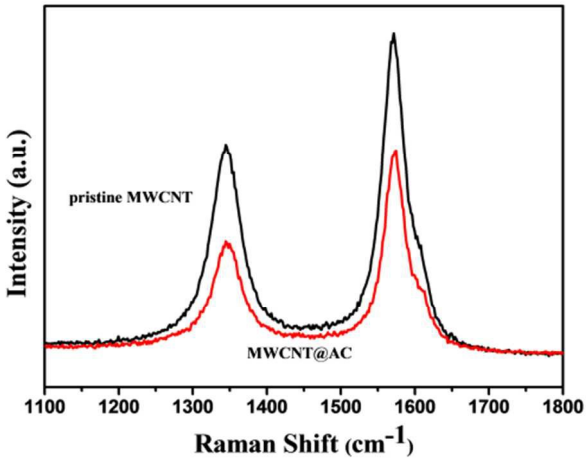

Fig. 3 Raman spectroscopy of pristine MWCNTs and MWCNT@AC nanohybrids.

The chemical structure of as-obtained MWCNT@AC nanohybrids and pristine MWCNTs were carefully characterized by FT-IR spectroscopy. As shown in Fig. 4, compared with pristine MWCNTs, there are no new peaks appearing in the spectroscopy of MWCNT@AC nanohybrids. However, the pristine MWCNTs precipitate rapidly in ethanol while MWCNT@AC nanohybrids have good dispersion stability. The improvement of dispersibility of MWCNT@AC nanohybrids can be attributed to the isolation effect of amorphous carbon shell. Due to the strong π-π interaction between adjacent MWCNTs, the pristine MWCNTs are prone to aggregate together resulting in a rapid precipitation in solution. After coated with amorphous carbon shell, the nearest distance (>4 nm) between adjacent MWCNTs is larger than the action range of π-π interaction. Therefore, the π-π interaction between MWCNT@AC has been significantly reduced. As a result, the MWCNT@AC nanohybrids can be dispersed in solvent homogeneously. Fig. 5 shows the typical SEM images of the composite sections. It indicates that MWCNT@AC nanohybrids are well dispersed in the PVDF matrix, whereas many MWCNT aggregates are clearly viewed in the MWCNT/PVDF composites.

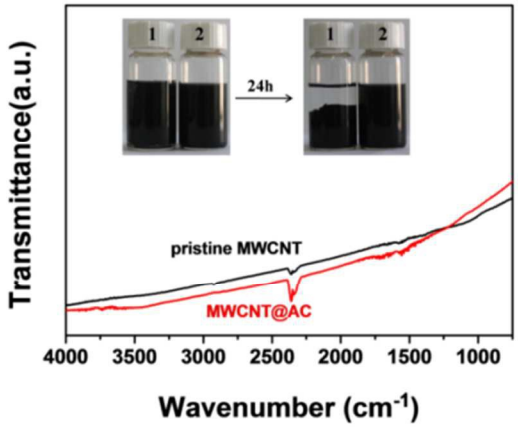

Fig. 4 FT-IR of pristine MWCNTs and MWCNT@AC nanohybrids. The inset showing the photographs of solution (ethanol) stability of the suspension with pristine MWCNTs and MWCNT@AC nanohybrids.

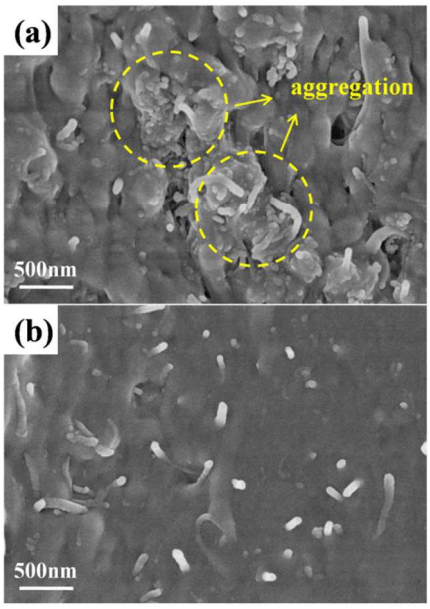

Fig. 5 SEM images of (a) pristine MWCNT/PVDF composites and (b) MWCNT@AC/PVDF composites.

2.3 Electrical conductivity

Electrical transport in polymer-based composites can occur either through direct contact between conductive fillers or tunneling of electrons between the sufficiently close conductive particles.[35] Fig. 6a and 6b show the frequency dependence of ac conductivity of MWCNT@AC/PVDF and pristine MWCNT/PVDF composites with different filler contents. At low concentrations, the conductivity of composites increases with increasing concentration. In this case, the conductive fillers are not contacting with each other so that the tunneling mechanism is dominant in the electronic transport. Hua et al.[36] reported that the tunneling conductivity of adjacent MWCNTs is related to the distance between MWCNTs. Therefore, the increase of conductivity with concentration can be attributed to the decreasing distance between MWCNTs. Besides, the strong frequency dependence of conductivity indicates that the composites show an insulating nature at low concentrations. With further increasing filler concentration, once exceeding the percolation

threshold, the conductivity values are almost independent of frequency in the low-frequency range because of the formation of conductive network. In this case, the composites show a conducting nature and the electrons can transport like in a typical inherently conducting material.

As shown in Fig. 6c, the conductivity values of two composites at same filler concentration show greatly difference. For instance, when the filler content is 1.5 vol%, the conductivity value of MWCNT/PVDF composites is approximately four orders of magnitude larger than that of MWCNT@AC/PVDF composites. In MWCNT/PVDF composites, a conductive network has been formed at a low concentration (<1.5 vol%) due to the direct contact of MWCNTs. Electrons can transport along the conductive network from one electrode to another like in conducting materials. However, the introduction of amorphous carbon shell prevents the direct contact of MWCNTs, making it difficult to form a conductive network in MWCNT@AC/PVDF composites. In this case, electrons can only transport through adjacent MWCNTs by inter-MWCNT tunneling. Therefore, the conductivity of MWCNT@AC/PVDF composites is much lower than that of MWCNT/PVDF composites with same filler contents.

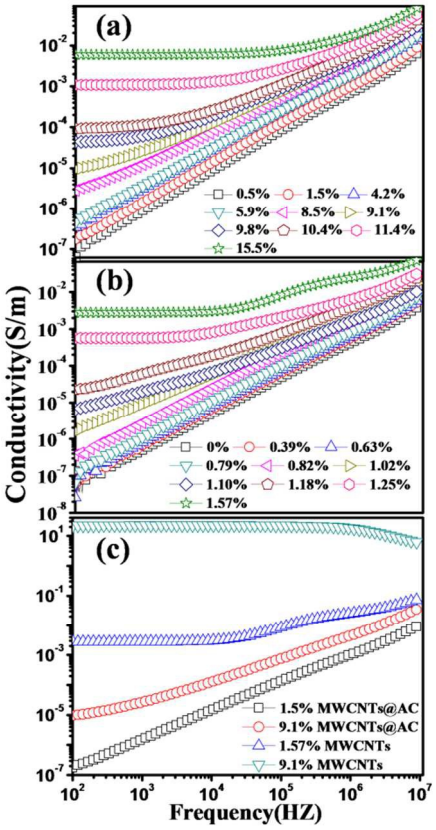

Fig. 6 Frequency dependence of the ac conductivity of (a) MWCNT@AC/PVDF composites and (b) pristine MWCNT/PVDF composites at different filler volume contents. (c) Ac conductivity comparison between MWCNT@AC/PVDF composites and pristine MWCNT/ PVDF composites.

Fig. 7 shows the ac conductivity of MWCNT@AC/PVDF and MWCNT/PVDF composites as a function of filler volume fraction, measured at room temperature and 1 kHz. In polymer-based composites, the volume fraction of the conductive fillers at the percolation threshold is the critical parameter for the electrical properties.[26] The following law can be used to explain the significant changes in the electrical properties near the percolation threshold:

$$\sigma_{eff} \propto \sigma_i (f_c - f)^{s}, \text{ for } f_c > f \quad (1)$$

Where σ_{eff} is the effective conductivity of composites, σ_i is the conductivity of insulating PVDF polymer, f_c is the percolation threshold, f is the volume fraction of fillers, s is the critical exponent in the insulating region. The best linear fits of the conductivity data to the log-log plots of the power laws for Equation (1) gave f_c=8.53 and s=1.71 for MWCNT@AC/PVDF composites and f_c=1.01 and s=0.64 for MWCNT/PVDF composites (see the inset in Fig. 7). The percolation threshold of MWCNT@AC/PVDF composites is much higher than that of MWCNT/PVDF composites due to the isolation effect of amorphous carbon shell, which makes it more difficult to form conductive network in MWCNT@AC/PVDF composites.

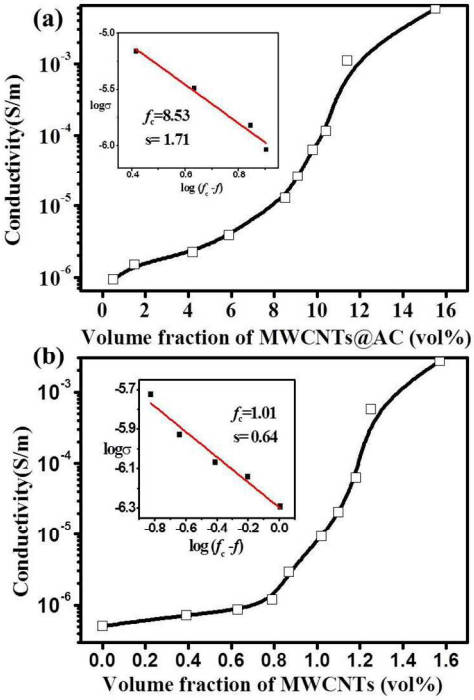

Fig. 7 Ac conductivity of (a) MWCNT@AC/PVDF and (b) pristine MWCNT/PVDF composites as a function of fillers volume fraction, measured at 1 kHz and room temperature. Their insets show the best fits of the conductivity to Eqs. (1) .

The different critical exponent s of two composites can be explained by Swiss-cheese model, which is based on a system constructed of conducting fillers embedded in insulting matrix. The model could apply to our composites with $f<f_c$, where the conduction process is controlled by inter-MWCNT tunneling.[25] The value of s is related to the average distance between adjacent MWCNTs. Because of the incorporation of amorphous carbon shell, the average distance will become larger relatively resulting in a larger s.

2.4 Dielectric properties

Fig. 8 shows the frequency dependence of dielectric constant of

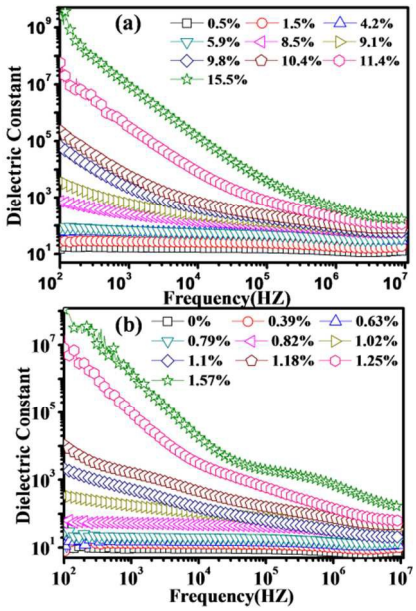

Fig. 8 Frequency dependence of the dielectric constant of (a) MWCNT@AC/PVDF composites and (b) pristine MWCNT/PVDF composites with difference filler volume contents.

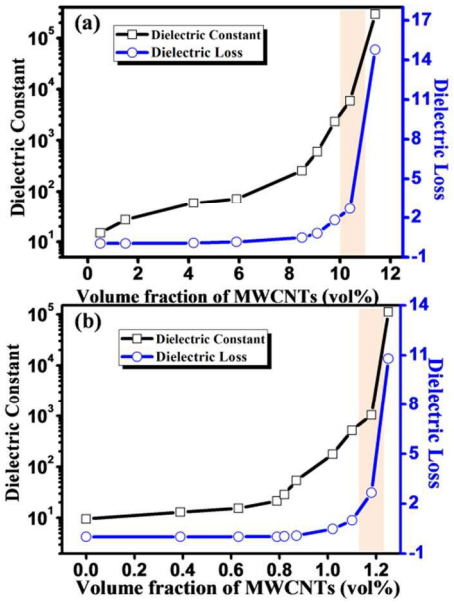

Fig. 9 Dielectric constant and dielectric loss of (a) MWCNT@AC/PVDF and (b) pristine MWCNT/PVDF composites as a function of fillers volume fraction, measured at 1 kHz and room temperature.

MWCNT@AC/PVDF and MWCNT/PVDF composites with different filler volume contents. When $f<f_c$, the dielectric constant decreases very slowly with the increase of frequency. As the filler content increases, the frequency dependence of dielectric constant becomes gradually stronger. When $f>f_c$, the dielectric constant exhibits a strong frequency dependence in the low-frequency range, followed by a weak frequency dependence in the high-frequency range, suggesting that interfacial polarization is dominant for the capacitance of these microcapacitors. [19,25]

Fig. 9 shows the dielectric constant and dielectric loss of MWCNT@AC/PVDF and MWCNT/PVDF composites as a function of filler content, measured at 1 kHz and room temperature. A common feature that can be seen in both composites is that the addition of conductive fillers increases the dielectric constant of composites, which is consistent with other polymer-based composites.[10,19,28] This can be well explained by the microcapacitor theory, which has been mentioned before. In detail, the evolution process of the dielectric permittivity can be divided into three stages. When $f<f_c$, a small amount of conductive fillers is incorporated into polymer matrix and isolated to each other. The capacitance of each microcapacitor is very low and the number of microcapacitors is inadequate, resulting in a slight increase of dielectric permittivity. As the volume fraction of nanofillers increases, once the volume fraction reaches percolation threshold fc where the nanofillers are close to each other, the dielectric permittivity of composites undergoes a sharp increase. This can be attributed to the formation of large number of microcapacitors and the increase of the capacitance of each microcapacitor. When the volume fraction is beyond f_c, the dielectric permittivity of composites keeps increasing because of the continuous formation of microcapacitors. Meanwhile, the dielectric loss is increased dramatically due to the formation of conductive network and the resultant leakage current within the composites. In this case, the composites turn to conducting materials rather than dielectrics.

From Fig. 9, we can observe that the dielectric constant of MWCNT@AC/PVDF composites reaches 5910 when the dielectric loss is about 2, which is about 5 times higher than that of MWCNT/PVDF composites (ε=1040). The great difference in dielectric constant between two composites can be attributed to the introduction of amorphous carbon shell around the surface of MWCNTs in MWCNT@AC/PVDF composites, which makes the direct contact of MWCNTs impossible. Compared to MWCNT/PVDF composites, more conductive fillers could be incorporated in MWCNT@AC/PVDF composites before the formation of conductive network. Accordingly, the percolation threshold of MWCNT@AC/PVDF composites has been significantly increased from 1.01 to 8.53. The increase in MWCNTs contents not only increases the number of microcapacitors but also increases the capacitance of each microcapacitor by decreasing the distance between two electrodes. As a result, the dielectric constant of MWCNT@AC/PVDF composites can be greatly enhanced. Meanwhile, the dielectric loss caused by the leakage current among adjacent MWCNTs can be significantly reduced because of the isolation effect of amorphous carbon shell. Fig. 10 shows the Bar chart comparing the dielectric constant and corresponding dielectric loss reported in the literature using polymer as a matrix in polymer-based composites.[16,19,22,25,28] The result shows that MWCNT@AC/PVDF composite has much better dielectric performance than the reported CNT/polymer composites before.

3 Conclusions

In conclusion, we have prepared a novel MWCNT@AC/PVDF composite by employing a core/shell structured MWCNT@AC nanohybrid as conductive filler. Compared to MWCNT/PVDF composites, gigantic enhancement in dielectric properties are achieved in MWCNT@AC/PVDF composites. We suggest that the excellent dielectric properties originate from the introduction of

amorphous carbon shell around the surface of MWCNTs. The ultrathin amorphous carbon shell provides a barrier layer between adjacent MWCNTs in polymer matrix, which not only prevents the direct contact of MWCNTs but also improves the dispersibility of MWCNTs. Such composites could be ideal dielectric materials for high-energy-density capacitors and the design concept used in our work can be extended to other carbon materials, such as carbon fiber and graphene.

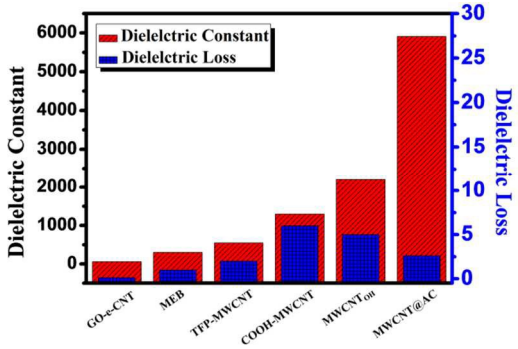

Fig. 10 Bar chart comparing the dielectric constant and corresponding dielectric loss reported in the literature using polymer as a matrix in polymer-based composites. [16,19,22,25,28]

4 Experimental

4.1 Fabrication of MWCNT@AC Nanohybrids

The core/shell structured MWCNT@AC nanohybrids were synthesized via a hydrothermal condition (HTC). The MWCNTs (purity > 97 wt%, diameter 40-60 nm, length 5-15 μm, density 2.25 g/cm^3) and monosaccharide D-(+)-Glucose were purchased from Aladdin Chemistry Co. Ltd. Briefly, pristine MWCNTs (60 mg) and two drops of triton were suspended in deionized water (60 mL) for 2 h with the ultrasonicator. Then glucose power (1.5 g) was added into the solution for another 1 h to form a homogeneous solution. The solution was then transferred in a rotating Teflon-sealed autoclave (100 mL, 3 r/min) and kept at 453 K for 12 h. After cooled in air naturally, the color of the solution changed from black to dark brown because of the carbonization and polymerization of glucose. The products were isolated by centrifugation, cleaned by three cycles of centrifugation/washing/redispersion in water and alcohol, and dried overnight in vacuum at 353 K. Finally, the resultant brown powders were heated to 573 K in nitrogen atmosphere for 2 h to immobilize the amorphous carbon shell on the surface of MWCNTs and reduce the cross linking sites between adjacent shells.

4.2 Preparation of Composites

MWCNT@AC/PVDF composites and MWCNT/PVDF composites, with different filler loadings, were produced by simple blending and subsequent molding. A desired amount of MWCNT@AC nanohybrids or MWCNTs was firstly dispersed in ethanol solution (20 mL) by ultrasonic treatment for 3 h. Subsequently, a certain amount of PVDF powder was dissolved in this suspension for another 2 h. Then the suspension was dried at 353 K for 4 h and grinded into fine powder. Finally, the composite powder was cold pressed to disk-shape sample with 15 mm in diameter and 1-1.5 mm in thickness at 20 MPa and kept at 493 K for 3 h.

4.3 Characterization

Fourier transform infrared spectra were measured using a Nicolet Nexus FTIR spectrometer by incorporating the sample in a KBr disk. The Raman spectrum was recorded on a JY LABRAM-HR Laser Micro Raman Spectrometer excited by a laser with 514.5 nm wavelength. The microstructures of MWCNT@AC nanohybrids were analyzed by using transmission electron microscopy (TEM, JEM-2100 UHR). For electric measurement, all samples were polished and painted with silver paste on both sides of the disk-shape samples. The conductivity, dielectric constant, and dielectric loss of the samples were measured by a HP 4194A precision impedance analyzer (Agilent Technologies, Inc.) at room temperature.

Acknowledgements

This work is supported by the Natural Science Foundation of China (11374372), Taishan Scholar Foundation (ts20130929) , the Fundamental Research Funds for the Central Universities (13CX05004A, 13CX05009A), Graduate Innovation Fund of China University of Petroleum (YCX2014070).

References

1 J. W. Shang, Y. H. Zhang, L. Yu, X. L. Luan, B. Shen, Z. L. Zhang, F. Z. Lv, P. K. Chu, *J. Mater. Chem. A*, 2013, **1**, 884.
2 R. Schroeder, L. A. Majewski, M. Grell, *Adv. Mater.,* 2005, **17**, 1535.
3 J. R. Miller, R. A. Outlaw, B. C. Holloway, *Science*, 2010, **329**, 1637.
4 M. S. Whittingham, *MRS Bull.*, 2008, **33**, 411.
5 P. Barber, S. Balasubramanian, Y. Anguchamy, S. Gong, A. Wibowo, H. Gao, H. J. Ploehn, H. C. zur Loye , *Materials*, 2009, **2**, 1697.
6 Q. Wang , L. Zhu, *J. Phys. D: Appl. Phys.*, 2011, **49**, 1421.
7 P. Kim, S. C. Jones, P. J. Hotchkiss, J. N. Haddock, B. Kippelen, S. R. Marder, J. W. Perry, *Adv. Mater.*, 2007, **19**, 1001.
8 H. Tang, Y. Lin, H. A. Sodano, *Adv. Energy Mater.*, 2012, **2**, 469.
9 L. Xie, X. Huang, C. Wu, P. Jiang, *J. Mater. Chem.*, 2011, **21**, 5897.
10 C. Yang, Y. Lin, C. W. Nan, *Carbon*, 2009, **47**, 1096.
11 M. N. Almadhoun, M. N. Hedhili, I. N. Odeh, P. Xavier, U. S. Bhansali, H. N. Alshareef, *Chem. Mater.*, 2014, **26**, 2856.
12 L. Qi, B. I. Lee, S. Chen, W. D. Samuels, G. J. Exarhos, *Adv. Mater.*, 2005, **17**, 1777.
13 C. Brosseau, F. Boulic, P. Queffelec, C. Bourbigot, Y. Le Mest, J. Loaec, A. Beroual, *J. Appl. Phys.*, 1997, **81**, 882.
14 J. Y. Kim, W. H. Lee, J. W. Suk, J. R. Potts, H. C, I. N. Kholmanov, R. D. Piner, J. Lee, D. Akinwande, R. S. Ruoff, *Adv. Mater.*, 2013, **25**, 2308.
15 S. Kirkpatrick, *Rev. Mod. Phys.*, 1973, **45**, 574.
16 Q. Li, Q. Z. Xue, L. Z. Hao, X. L. Gao, Q. B. Zheng, *Compos. Sci. Technol.*, 2008, **68**, 2290.
17 Z. M. Dang, J. K. Yuan, J. W. Zha, T Zhou, T. L. Sheng, G. H. Hu, *Prog. Mater. Sci.*, 2012, **57**, 660.
18 T. B. Adams, D. C. Sinclair, A. R. West, *Adv. Mater.*, 2002, **14**, 1321.
19 C. Wu, X. Y. Huang, X. F. Wu, L. Y. Xie, K. Yang, P. K. Jiang, *Nanoscale*, 2013, **5**, 3847.
20 C. W. Nan, Y. Shen, J. Ma, *Annu. Rev. Mater. Res.*, 2010, **40**, 131.
21 I. Alig, D. Lellinger, M. Engel, T. Skipa, P. Pötschke, *Polymer*, 2008, **49**, 1902.
22 R. R. Kohlmeyer, A. Javadi, B. Pradhan, S. Pilla, K. Setyowati, J. Chen, S. Gong, *J. Phys. Chem. C*, 2009, **113**, 17626.
23 A. B. Dichiara, J. K. Yuan, S. H. Yao, A. Sylvestre, L. Zimmer and J. Bai,

J. Mater. Chem. A, 2014, **2**, 7980.
24 L. Wang, Z. M. Dang, *Appl. Phys. Lett.*, 2005, **87**, 042903.
25 Z. M. Dang, L. Wang, Y. Yin, Q. Zhang, Q. Q. Lei, *Adv. Mater.*, 2007, **19**, 852.
26 V. Datsyuka, M. Kalyvaa, K. Papagelisb, J. Partheniosa, D. Tasisb, A. Siokoua, I. Kallitsisa, C. Galiotis, *Carbon*, 2008, **46**, 833.
27 L. Y. Chu, Q. Z. Xue, J. Sun, F. J. Xia, W. Xing, D. Xia, M. D. Dong, *Compos. Sci. Technol.*, 2013, **86**, 70.
28 T. Zhou, J. W. Zha, Y. Hou, D. Wang, J. Zhao, Z. M. Dang, *ACS Appl. Mater. Interfaces*, 2011, **3**, 4557.
29 Y. Q. Lin, A. Dichiara, D. L. He, P. Haghi-Ashtiani, J. B. Bai, *Chem. Phys. Lett.*, 2012, **554**, 137.
30 A. Dichiara, Y. Lin, D. He, J. Bai. Sci. *Adv. Mater.*, 2014, **6**, 377.
31 X. M. Sun, Y. D. Li, *Angewandte Chemie Int. Ed.*, 2004, **43**, 597.
32 H. S. Qian, S. H. Yu, L. B. Luo, J. Y. Gong, L. F. Fei, X. M. Liu, *Chem. Mater.*, 2006, **18**, 2102.
33 Q. Z. Xue, X. Zhang, *Carbon*, 2005, **43**, 760.
34 J. Yang, J. T. Chen, S. X. Yu, X. B. Yan, Q. J. Xue, *Carbon*, 2010, **48**, 2644.
35 N. Yousefi, X. Y. Sun, X. Y. Lin, X. Shen, J. J. Jia, B. Zhang, B. Z. Tang, M. S. Chan, J. K. Kim, *Adv. Mater.*, 2014, **26**, 5480.
36 N. Hua, Y. Karubea, C. Yan, Z. Masudaa, H. Fukunaga, *Acta Mater.*, 2008, **56**, 2929.